A New Method of Accurate Broken Rotor Bar Diagnosis based on Modulation Signal Bispectrum Analysis of Motor Current Signals

F. Gu[1,2], T. Wang[2], A. Alwodai[1], X. Tian[1], Y. Shao[3], A.D. Ball[1]

[1]University of Huddersfield, Queensgate, Huddersfield, HD1 3DH, UK

[2] Taiyuan University of Technology, Taiyuan, Shanxi, China

[3]State Key Laboratory of Mechanical Transmission, Chongqing University, Chongqing, China

Corresponding author: f.gu@hud.ac.uk

Abstract

Motor current signature analysis (MCSA) has been an effective way of monitoring electrical machines for many years. However, inadequate accuracy in diagnosing incipient broken rotor bars (BRB) has motivated many studies into improving this method. In this paper a modulation signal bispectrum (MSB) analysis is applied to motor currents from different broken bar cases and a new MSB based sideband estimator (MSB-SE) and sideband amplitude estimator are introduced for obtaining the amplitude at $(1\pm 2s)f_s$ (s is the rotor slip and f_s is the fundamental supply frequency) with high accuracy. As the MSB-SE has a good performance of noise suppression, the new estimator produces more accurate results in predicting the number of BRB, compared with conventional power spectrum analysis. Moreover, the paper has also developed an improved model for motor current signals under rotor fault conditions and an effective method to decouple the BRB current which interferes with that of speed oscillations associated with BRB. These provide theoretical supports for the new estimators and clarify the issues in using conventional bispectrum analysis.

Keywords: Induction motors, conventional bispectrum, modulation signal bispectrum, motor current signal model, broken rotor bar.

1 INTRODUCTION

Induction motors are the most widely used prime movers in industry. Broken rotor bars (BRB) in motors are a common fault which often brings unexpected breakdowns and leads to loss of productivity. In recent years, this type of fault has been increasingly studied for developing advanced

techniques that permit on-line early detection and diagnosis of motor faults to avoid any negative consequences of unexpected shutdowns.

As the main stream technique, signature analysis of motor phase current (MCSA) based on spectrum amplitude, has been widely used to detect BRB and end ring faults. The sideband components at frequency $(1 \pm 2ks) f_s$ have been used to detect such faults, (*s* is the rotor slip and f_s is the supply frequency, and harmonic integer *k*=1, 2, 3,… n). In particular, the amplitudes at these sideband components are tested to estimate the number of BRB for diagnosing the severity of the problem. Although, the MCSA gives acceptable detection results, its diagnostic method on a number of BRBs has not yet had a unified method. As shown in the review papers [1, 2] there are more than 5 formulae suggested by different researchers to predict the number of BRB based sideband amplitudes from spectrum analysis.

One of the causes of this inconsistency may stem from the inherent drawbacks of noise inclusion in discrete Fourier transform (DFT) based spectrum analysis. To obtain more accurate results new signal processing methods have been tried in many of the latest studies. Of particular interest is the work to perform diagnosis to involve the phase information from DFT. In [3] the phase, rather than the modulus, of DFT of current signals was explored for broken rotor bar detection, The results show the phase of DFT allows the detection of one broken rotor bar when the motor operates under a low load (25% of rated load) but the robustness of the method decreases in the case of the half-broken rotor bar.

Furthermore, Saidi, et al [4] tried to use the diagonal slices of a conventional bispectrum(CB) applied to stator current signals, which is a good attempt at combining the information from both the modulus and phase for BRB detection through CB. They claim that the results are superior in the accurate detection of rotor broken bars even when the induction machine is rotating at a very low level of shaft load (no-load condition). However, it is a dubious claim because the bispectrum slices show unconvincing peaks at the sidebands even under the load of 25%. In addition, the bispectrum estimation is obtained by using only four averages, which is certainly not enough to obtain a reliable estimation from the statistical point of view.

On the other hand, an earlier study by the authors[5] on using motor current signals for the diagnosis of different faults, has in reciprocating compressors, revealed that by suppressing random noise with a new data processing method, named as modulation signal bispectrum (MSB) which is an extension of CB for analysing modulation signals particularly, has resulted in more accurate diagnosis than that of power spectrum(PS). This shows that MSB is an effective method used to detect and quantify sidebands in current signals through its high performance of noise suppression. The application of MSB is fully supported by the signal model developed in the paper. Following the success of using

MSB for reciprocating compressors, the method has been further improved so that the MSB slice which excludes carrier amplitudes is developed to achieve a fast calculation of MSB and to compare it directly with PS, which has led to good results in detecting and diagnosing different faults from multi-stage gearboxes and electrical motors [6-9]. However, these applications rely on the combination of the sideband product obtained from the MSB. It has not been tried to separate the product explicitly into their individual components which are usually required for BRB severity diagnosis [10-18].

To use MSB for obtaining more accurate results in diagnosing BRB, this paper develops a new MSB based sideband amplitude estimator (MSB-SE) that allows the amplitudes at lower and higher sidebands of $(1 \pm 2s) f_s$ to be estimated individually and the BRB current component to be decoupled from motor current signals with inevitable noise and interferences. Following this introduction, the contents in this paper have further five sections. Section 2 derives the signal model due to BRB to include phase components to pave a theoretical base for applying MSB analysis. Section 3 extends MSB analysis so that the new MSB-SE is developed to accurately predict the amplitude of sidebands for predicting the number of BRB with a higher accuracy. Section 4 details experimental facilities and methods to evaluate these new methods. Section 5 presents the results and discussion. Finally section 6 gives the key conclusions drawn in this study.

2 MOTOR CURRENT SIGNAL MODEL FOR A FAULTY ROTOR

A signal model for BRB has been presented in [10,11] to explain the roots of sideband components at $(1 \pm 2s) f_s$. By following the developing process of the model, this section extends the model to include phase effects, which provide a foundation for applying MSB to motor current signals and developing a reliable way for sideband extraction.

2.1 Current signal under healthy conditions

When a motor drive is operating under healthy conditions, the ideal electromagnetic relationship of the driving motor can be examined in just one of the three phases, for example phase *A,* for an easier understanding of the effect due to asymmetric rotor fault such as a broken rotor bar. By neglecting the higher order harmonics and inherent errors and referring to supply voltage signal, the current signal in phase *A* for a healthy motor drive can be expressed as

$$i_A = \sqrt{2} I \cos(2\pi f_s t - \alpha_I) \tag{1}$$

Correspondingly, the magnetic flux in the motor stator is

$$\phi_A = \sqrt{2} \phi \cos(2\pi f_s t - \alpha_\phi) \tag{2}$$

The electrical torque produced by the interaction between the current and flux can be expressed as

$$T = 3P\phi I \sin(\alpha_I - \alpha_\phi) \tag{3}$$

where I and ϕ denote the root mean squared (RMS) amplitudes of the supply current and the linkage flux respectively, α_I and α_ϕ are the phases of the current and flux respectively referring to supply voltage, f_s is the fundamental frequency of electrical supply and P is the number of pole pairs.

2.2 Current signal under broken rotor bar

If there is a fault on the rotor such as a broken rotor bar, there will be an additional current component, denoted as, i_f in the stator winding due to interaction between the main magnetic fields between stator and rotor [10,11]. Supposing that the additional current is a sinusoidal wave with a frequency $f_F = 2sf_s$ for the case of BRB, an associated current wave with a BRB amplitude I_F and phase angle α_F, referring to the supply voltage, can be expressed as

$$i_f = \sqrt{2} I_F \cos(2\pi f_F t - \alpha_F) \tag{4}$$

Correspondingly, an oscillatory electric torque due to its interaction with the fundamental flux can be derived using electric torque equation $T_e = \mathrm{Im}(P\vec{\phi}\,\vec{I}_F^{\,*})$ as

$$\Delta T = 3P\phi I_F \sin[2\pi f_F t - \alpha_\phi + \alpha_F] \tag{5}$$

which causes the motor rotor to produce a corresponding angular speed oscillation due to $J\frac{d}{dt}(\Delta\omega / P) = \Delta T$ and hence angular displacement oscillation is

$$\Delta\theta(t) = \int \Delta\omega dt = -\frac{3P^2\phi I_F}{4\pi^2 f_F^2 J}\sin[2\pi f_F t - \alpha_\phi + \alpha_F] \tag{6}$$

where *J* is the inertia of the rotor system of the motor. This angular oscillation modulates the phase of the linkage flux in Eqn. (2) and yields

$$\begin{aligned}\phi_A^F &= \sqrt{2}\phi\cos[2\pi f_s t - \alpha_\phi + \Delta\theta(t)] \\ &\approx \sqrt{2}\phi\cos(2\pi f_s t - \alpha_\phi) + \sqrt{2}\Delta\phi_F \cos[2\pi(f_s - f_F)t - \alpha_F] \\ &\quad - \sqrt{2}\Delta\phi_F \cos[2\pi(f_s + f_F)t - 2\alpha_\phi + \alpha_F]\end{aligned} \tag{7}$$

where $\Delta\phi_F = \frac{3P^2\phi^2 I_F}{4\pi^2 f_F^2 J}$.

The derivative of the first term of the flux is the fundamental electromotive force (EMF), while the derivative of the other two terms produces two new EMFs:

$$\begin{aligned} E_A^F &= -\sqrt{2}\phi 2\pi f_s \sin(2\pi f_s t - \alpha_\phi) \\ &-\sqrt{2}\Delta\phi_F 2\pi(f_s - f_F)\sin[2\pi(f_s - f_F)t - \alpha_F] \\ &+\sqrt{2}\Delta\phi_F 2\pi(f_s + f_F)\sin[2\pi(f_s + f_F)t - 2\alpha_\phi + \alpha_F] \end{aligned} \tag{8}$$

If the equivalent winding impedance at supply frequency is $z = Ze^{\alpha_\phi}$ and assuming that it changes with frequency shifts relative to the supply frequency, the impedances at the two sideband components are $z_l = (Z - \Delta Z_l)e^{(\varphi_Z + \Delta\varphi_{Zl})}$ and $z_r = (Z + \Delta Z_r)e^{(\varphi_Z - \Delta\varphi_{Zr})}$, which means that the modulus of impedance increases with the increase in frequency and the phase decreases with frequency. These EMFs will lead to new motor currents as follows:

$$\begin{aligned} i_A^{FS} &= -\frac{\sqrt{2}\phi 2\pi f_s}{Z}\sin(2\pi f_s t - \alpha_\phi - \alpha_Z) \\ &-\frac{\sqrt{2}\Delta\phi_F 2\pi(f_s - f_F)}{Z - \Delta Z_l}\sin[2\pi(f_s - f_F)t - \alpha_F - \varphi_Z - \Delta\varphi_{Zl}] \\ &+\frac{\sqrt{2}\Delta\phi_F 2\pi(f_s + f_F)}{Z + \Delta Z_r}\sin[2\pi(f_s + f_F)t - 2\alpha_\phi + \alpha_F - \varphi_Z + \Delta\varphi_{Zr}] \end{aligned} \tag{9}$$

The difference between ΔZ_l and ΔZ_r becomes larger with the increase in loads due to the increase in slip and so do the two phases. In addition, for higher order harmonics, these effects will be more significant. So this change is kept in this study to explain the asymmetric sidebands in the spectrum when large frequency shifts are examined for rotor misalignments, which is approximately a 50% difference relative to the fundamental, rather than not taken into account as in [11, 12].

Combining Eqn. (4) with Eqn. (9) yields the final current signal under rotor faulty conditions:

$$\begin{aligned} i_A^F &= i_A^{FS} + i_f \\ &= \sqrt{2}I\sin(2\pi f_s t - \alpha_\phi - \varphi_Z) \\ &+\sqrt{2}I_F\cos[2\pi(f_s - f_F)t - \alpha_F] \\ &+\sqrt{2}I_{Fl}\sin[2\pi(f_s - f_F)t - \alpha_F - \varphi_Z - \Delta\varphi_{Zl}] \\ &-\sqrt{2}I_{Fr}\sin[2\pi(f_s + f_F)t - 2\alpha_\phi + \alpha_F - \varphi_Z + \Delta\varphi_{Zr}] \end{aligned} \tag{10}$$

where $I_{Fl} = 2\pi(1-2s)f_s\,\Delta\phi/(Z - \Delta Z)$ and $I_{Fr} = 2\pi(1+2s)f_s\,\Delta\phi/(Z + \Delta Z)$ are the modulus of sideband components due to speed oscillations which are caused originally by BRB currents in Eqn.

(4). It shows that the current signal of the faulty case exhibits three new additional components, compared with that of a normal operation. Two of these are the lower sideband components at the same frequency, but with different phases, and the other is the upper sideband component with a phase different from the previous two. To see the possible connection of these components Eqn. (10) can be expressed using phase shift relationships: $\cos(\pi/2+\theta)=-\sin(\theta)$ and $\cos(\pi+\theta)=-\cos(\theta)$

$$\begin{aligned} i_A^F &= \sqrt{2}I\cos(2\pi f_s t-\alpha_\phi-\varphi_Z+\pi/2+\pi) \\ &+\sqrt{2}I_F\cos[2\pi(f_s-f_F)t-\alpha_F] \\ &+\sqrt{2}I_{Fl}\cos[2\pi(f_s-f_F)t-\alpha_F-\varphi_Z-\Delta\varphi_{Zl}+\pi/2+\pi] \\ &+\sqrt{2}I_{Fr}\cos[2\pi(f_s+f_F)t-2\alpha_\phi+\alpha_F-\varphi_Z+\Delta\varphi_{Zr}+\pi/2] \end{aligned} \tag{11}$$

Furthermore, the two lower sidebands in Eqn.(11) can be combined to yield

$$i_l=\sqrt{2}\sqrt{I_F^2+I_{Fl}^2-2I_FI_{Fl}\sin(\phi_Z+\Delta\varphi_{Zl})}\cos[2\pi(f_s-f_F)t-\alpha_F-\delta] \tag{12}$$

where the amplitude of lower sideband in RMS value is

$$I_L=\sqrt{I_F^2+I_{Fl}^2-2I_FI_{Fl}\sin(\phi_Z+\Delta\varphi_{Zl})} \tag{13}$$

the phase angle is

$$\cos(\delta)=\frac{\sqrt{2}I_F-\sqrt{2}I_{Fl}\sin(\varphi_Z+\Delta\varphi_{Zl})}{\sqrt{2I_F^2+2I_{Fl}^2-4I_FI_{Fl}\sin(\phi_Z+\Delta\varphi_{Zl})}} \tag{14}$$

It shows that the lower sideband amplitude appearing in PS is combined from two different types of underlying physical processes. Alternatively, the BRB current interferes with the current component due to speed oscillation.

Substituting Eqn. (12) into i_A^F in Eqn. (11) yields a more concise expression of the current signal for asymmetrical rotor faults:

$$\begin{aligned} i^F{}_A &\approx \sqrt{2}I\cos(2\pi f_s t-\alpha_\phi-\varphi_Z+\pi/2+\pi) \\ &+\sqrt{2}I_L\cos[2\pi(f_s-f_F)t-\alpha_F-\delta] \\ &+\sqrt{2}I_{Fr}\cos[2\pi(f_s+f_F)t-2\alpha_\phi+\alpha_F-\varphi_Z+\Delta\varphi_{Zr}+\pi/2] \end{aligned} \tag{15}$$

From the above derivation and discussion it can be concluded that:

1) The BRB leads to additional current components which will be the lower and upper sideband components at $(1\pm 2s)f_s$ shown in the spectrum of motor current signal.

2) The amplitudes of these sidebands are influenced by rotor inertia, load variation, power factor and machine impedance. Especially, the amplitude of the original BRB current i_f shown at the lower sideband interferes with that due to speed oscillations. This means that the interference needs to be eliminated to obtain the amplitude of i_f for accurate and reliable prediction of fault severity.
3) The phases of sidebands are not only related to the same factors as their amplitude, but also the phase variation of the fault current. However, it will be shown in Section 3 that an appropriate phase combination between sidebands and the carrier of fundamental supply can eliminate the phase variation in order to achieve reliable and accurate sideband estimation.

2.3 BRB fault current amplitude decoupling

To determine fault severity i.e. the number of BRB, the BRB current amplitude needs to be decoupled from the interference. For the first harmonic component at frequency $(1 \pm 2s) f_s$, the shift in frequency is relatively small with respect to the fundamental frequency. So the changes of impedance at the lower and upper sideband are close to each other and with a small change in amplitude. This means that the amplitudes of two sidebands due to speed oscillation will be equal and the changes of impedance ΔZ can be neglected to follow the assumption made in [11, 12]. Thus the amplitude of the lower sideband I_{Fl} in Eqn.(13) due to speed oscillation can be approximated by the upper sideband I_{Fr} and the amplitude of lower sideband in Eqn.(13) due to BRB can be repressed as:

$$I_{Lb} = \sqrt{I_F^2 + I_{Fr}^2 - 2 I_F I_{Fr} \sin(\phi_Z)} \tag{16}$$

With a known amplitude of the lower sideband and upper sideband from spectrum analysis, the power factor calculated from current measured at operating load and the power factor at rated current obtained from motor nameplates, the BRB current amplitude I_F can be estimated by solving the following quadratic equation:

$$I_F^2 - 2 I_{Fr} \sin(\phi_Z) I_F + I_{Fr}^2 - I_{Lb}^2 = 0 \tag{17}$$

In this way the interference of the speed oscillation can be decupled in the lower sideband, allowing fault severity to be obtained more correctly. However, reported works in the literature have not performed this key decoupling step in estimating the number of BRB [12-17], which is one of the main reasons that results in either overestimated or underestimated numbers of BRB.

3 Sideband Estimation using Modulation Signal Bispectrum

Section 2 shows that the current sideband components can be estimated using spectrum analysis. However, the amplitudes from conventional power spectrum include the additive random noise which is inevitable in measurement systems and motor operating process. To suppress noise, this section develops a new sideband amplitude estimator based on MSB analysis.

3.1 Modulation signal bispectrum (MSB)

For a discrete time current signal $x(t)$ its Discrete Fourier Transform (DFT) $X(f)$ is defined as:

$$X(f) = \sum_{t=-\infty}^{\infty} x(t) e^{-2j\pi t} \tag{18}$$

and the second-order measure of power spectrum (PS) of $x(t)$ can be estimated by the formula:

$$P(f) = E[X(f)X^*(f)] \tag{19}$$

where $X^*(f)$ is the complex conjugate of $X(f_1)$ and $E[\,]$ is the statistical expectation. The power spectrum is the popular method for current signal analysis because it can be calculated by fast Fourier transform(FFT). However, it contains only amplitude information of individual component f and ignores the effects of signal phases, leading to random noise inclusion. Extending this definition to the measures of order three gives rise to the estimation of CB:

$$B(f_1, f_2) = E[X(f_1)X(f_2)X^*(f_1 + f_2)] \tag{20}$$

CB of Eqn.(20) allows phase information between different component to be taken into account and shows unique performance in examining the presence of possible quadratic phase coupling (QPC) from the harmonically related frequency components of f_1, f_2 and $f_1 + f_2$. However, it neglects the possibility that the occurrence of $f_1 - f_2$, the lower sideband in PS, may be also due to the nonlinear relationship between the two components of f_1 and f_2. Because of this, it is not adequate to describe modulation signals such as the motor current signal in Eqn. (15). To improve the performance of CB in characterising the motor current signals, this study uses a modulation signal bispectrum (MSB) which has been investigated extensively by the authors in [5-9]:

$$B_{MS}(f_1, f_2) = E[X(f_2 + f_1)X(f_2 - f_1)X^*(f_2)X^*(f_2)] \tag{21}$$

Unlike the CB in Eqn.(20), this definition takes into account both $(f_1 + f_2)$ and $(f_1 - f_2)$ concurrently for characterizing the nonlinear coupling in modulation signals. It shows that a bispectral peak will be presented clearly at bifrequency $B_{MS}(f_1, f_2)$ if $(f_1 + f_2)$ and $(f_1 - f_2)$ are both due to

nonlinear coupling between f_1 and f_2. This is more accurate and effective in representing the modulation signals.

The overall phase of MSB in Eqn. (21) is

$$\phi_{MS}(f_1, f_2) = \phi(f_2 + f_1) + \phi(f_2 - f_1) - \phi(f_2) - \phi(f_2) \tag{22}$$

when two components f_1 and f_2 are coupled, their phases are related by

$$\begin{aligned} \phi(f_2 + f_1) &= \phi(f_2) + \phi(f_1) \\ \phi(f_2 - f_1) &= \phi(f_2) - \phi(f_1) \end{aligned} \tag{23}$$

By substituting (23) into (22) the total phase of MSB will be zero and its amplitude will be the product of the four magnitudes, which is the maximum of the complex product. Therefore, a bispectral peak will appear at (f_1, f_2). Eqn. (21) now includes both $(f_1 + f_2)$ and $(f_1 - f_2)$ simultaneously for measuring the nonlinearity of modulation signals. If $(f_1 + f_2)$ and $(f_1 - f_2)$ are both due to nonlinear effect between f_1 and f_2 a bispectral peak will appear at bifrequency (f_1, f_2). This is more accurate and apparent in representing the sideband characteristics of modulation signals.

With this definition, the MSB phase of BRB current signals presented in Eqn.(15) can be obtained as

$$\begin{aligned} \phi_{MS}(f_F, f_s) &= \phi(f_s + f_F) + \phi(f_s - f_F) - \phi(f_s) - \phi(f_s) \\ &= -2\alpha_\phi - \varphi_Z + \Delta\varphi_{Zr} + \pi/2 - \delta - 2(-\alpha_\phi - \varphi_Z + \pi/2 + \pi) \\ &= \varphi_Z + \Delta\varphi_{Zr} - \delta - \pi/2 \end{aligned} \tag{24}$$

Eqn.(24) shows that the MSB phase of current signals relates only to the machine parameters including the impedance phase $\varphi_Z + \Delta\varphi_{Zr}$ and fault amplitude induced phase δ, but not fault phase α_F and magnetic flux phase α_ϕ. This means that the phase of MSB will be a constant when the motor is operating under steady conditions. In other words, MSB is independent of the angular position of the motor rotor or the start point of a signal segment acquired. This will allow sufficient averages in MSB estimation to be performed using a data set collected or framed at any time through a Welch method. The average in turn will suppress random noise and non-modulating components to obtain a reliable estimation of MSB and of the hidden modulating signal.

It is worth noting that the phase of CB applied to signals expressed in Eqn. (15) is not independent of signal segments used. This means that an average process in estimating CB will lead to an uncertain result. Instead, it will change with segment sequences used, in an extreme case, CB magnitude will be

close to zeroes if the phases of data segments are distributed uniformly between 0 and 2π . Therefore, CB is not suitable for analyzing motor current signals.

In the case when the fault is due to pure speed oscillation, such as a misaligned shaft and rotor eccentricity, the MSB phase is simplified by excluding the second term in Eqn. (11) as

$$\phi_{MS}(f_F, f_s) = \Delta\varphi_{Zr} - \Delta\varphi_{Zl} - \pi \tag{24a}$$

i.e. the phase will be closer to π . Especially, when the impedance phase changes are in the sample amplitude, the MSB phase will be a constant value of π , showing that the modulation due to pure speed oscillation is close to the phase modulation process.

3.2 Sideband estimator using MSB

Because a motor current signal with electrical and mechanical faults contains a series of sideband components which appear mainly around the supply component, a bispectrum slice at the supply frequency will be sufficient to characterize these sidebands for fault detection and diagnosis. By setting f_2 in Eqn. (21) into a constant frequency value such as the fundamental $f_2 = f_s = 50\,\text{Hz}$, an MSB slice at supply frequency can be expressed as:

$$B_{MS}(f_1, f_s) = E[X(f_s + f_1)X(f_s - f_1)X^*(f_s)X^*(f_s)] \tag{25}$$

In fault diagnosis it is the amplitude of the sideband or modulator that is useful for both detection and diagnosis. However, the magnitude of $B_{MS}(f_1, f_s)$ from Eqn. (21) or (25) is a combination of sideband and supply components. The diagnostic results will be influenced by the amplitude at supply frequency, or the results are too sensitive to load conditions.

Considering that the amplitude of supply frequency is predominant in current signals and it can be identified easily in the frequency domain, an MSB slice based sideband estimator, abbreviated as MSB-SE, can be introduced as

$$B_{MS}^{SE}(f_1, f_s) = E[X(f_s + f_1)X(f_s - f_1)X^*(f_s)/|X(f_s)|\,X^*(f_s)/|X(f_s)|] \tag{26}$$

to quantify the combined effect of sidebands only, but not the carrier at the supply frequency. Because the magnitude of $X^*(f_s)/|X(f_s)|$ is unity, in the form of magnitude-phase, the sideband estimator is

$$B_{MS}^{SE}(f_1, f_s) = E[|X(f_s + f_1)\| X(f_s - f_1)|\, e^{j\phi_{MS}(f_1, f_s)}] \tag{27}$$

showing that the phase information of f_s is still taken into account in the estimation process and hence the noise suppression property is well maintained by MSB-SE.

Eqn. (26) and (27) show that the magnitude of MBS-SE peaks is determined purely by the magnitude product of sideband components. It means that the product of two symmetrical sidebands $|X(f_s+f_1)||X(f_s-f_1)|$ is equal to either $|X(f_s-f_1)||X(f_s-f_1)|$ or $|X(f_s+f_1)||X(f_s+f_1)|$ in the PS expression of Eqn. (19) provided that the two sidebands have the same amplitude and the signal is noise free. This shows that the unit of MSB-SE has the same unit as that of PS and hence they can be compared easily.

However, the amplitude from Eqn. (26) or (27) is obtained by including phase effects which highlights components with the same phases, and suppress any components with phase inconsistency such as random noise. On the other hand, the sideband amplitude from PS includes noise influences because the estimation of power spectrum does not take into account phase information. Therefore, it will have the relation in Eqn.(28) provided that the amplitudes of lower and upper sidebands are the same in a pure modulation signal such as those from AM and PM processes .

$$B_{MS}^{SE}(f_1, f_s) \le PS[|X(f_s+f_1)||X(f_s-f_1)|] \tag{28}$$

For the current signals of Eqn.(15), the relationship of Eqn.(28) may not be true because the two sidebands are not symmetric or have amplitude differences. Nevertheless, Eqn.(28) can be a reference for checking the degree of asymmetry and the correctness of the estimation process.

In addition, MSB-SE can also have its coherence function. According to [5] and Eqn.(26), MSB-SE coherence can be obtained by

$$b^2{}_{MSB-SE}(f_1, f_s) = \frac{|B_{MS}^{SE}(f_1, f_s)|^2}{E[|X(f_s+f_1)X(f_s-f_1)|^2]} \tag{29}$$

to confirm the coupling effects between sidebands and carrier and to check the degree of random noise influence, which allows confirmation of the existence of SMS-SE peaks for the detection of modulation process in noise measurements.

3.3 Sideband Amplitude Estimator based on MSB-SE

To reconstruct the amplitude of sidebands for more general cases when the two sidebands are not symmetric, the amplitude relationship between PS and MSB-SE embedded in Eqn. (26) can be used to give a more accurate estimation of the sideband amplitude with minimal noise influence. Assuming that the random noise has the same amplitude in the frequency bands around the carrier component, an estimation of sideband amplitudes $|\hat{X}_L|$ and $|\hat{X}_U|$ with minimal noise can be expressed through PS as

$$|\hat{X}_L| = X_L - \Delta \text{ and } |\hat{X}_U| = X_U - \Delta \tag{30}$$

where X_L and X_U are the root mean squared (RMS) amplitude of the lower and upper sidebands from PS estimation, and Δ is the noise amplitude which can be calculated based on the amplitude relationship of Eqn. (26) between PS and MSB-SE:

$$(X_L - \Delta)(X_U - \Delta) = \left| B_{MS}^{SE}\left(f_{2sf_s}, f_s\right) \right| \tag{31}$$

i.e. solving the following quadratic equation for the noise amplitude Δ

$$\Delta^2 - (X_L + X_U)\Delta + X_L X_U - \left| B_{MS}^{SE}\left(f_{2sf_s}, f_s\right) \right| = 0 \tag{32}$$

In this way, the estimated amplitude of sidebands will include minimal noise influences and produce a more accurate estimation of BRB severity.

4 TEST SETUP

To evaluate the current signal model and the performance of MSB-SE in diagnosing BRB of induction motors, an induction motor rig was used to acquire current data sets from four induction motors with the same specification, but three different degrees of BRB severity and a baseline motor. In the meantime these motors were also tested under different load conditions to evaluate the load dependency of the method.

4.1 Test facility

Fig. 1 shows the schematic of the test facilities employed to examine motor rotor faults. The system consists of an induction motor, variable speed controller, supporting bearings, couplings and DC generator as a load. The tested induction motor is a three-phase induction motor with rated output power of 4 kW at speed of 1420 rpm (two-pole pairs), 28 rotor bars and 36 stator slots, as detailed in Table 1.

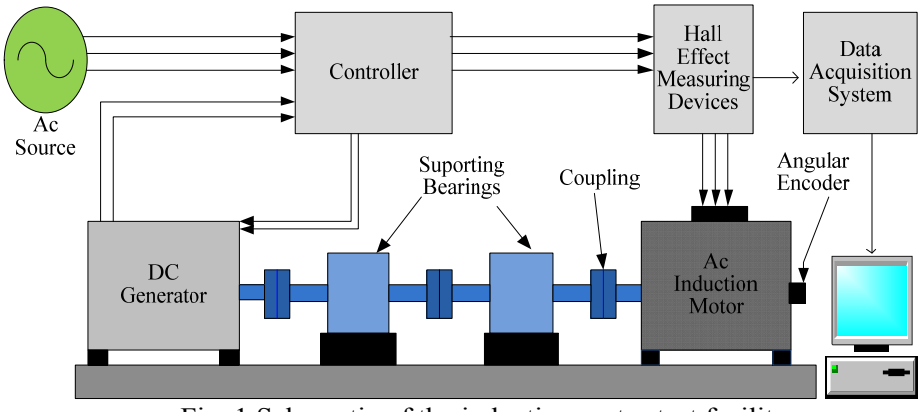

Fig. 1 Schematic of the induction motor test facility

4.2 Fault simulation

Three BRB cases with different BRB severities and one baseline case were tested with four motors of identical specification under the same operating conditions. As illustrated in Figure 2, the first BRB case is a motor with half BRB which was created by drilling a hole into one of the 28 bars up to the half depth of a bar. The second is one complete bar breakage created by drilling the hole to the full depth of the bar. And the third is two continuous bar breakage which was induced by drilling two bars side by side to their full depth as shown in Figure 2 (b). These three fault cases were induced in three different motors with the same specifications as shown in Table 1 and they were tested to have close baseline signatures before the faults were created on their rotors.

(a) Rotor with one bar breakage

(b) Rotor with two bar breakage

Fig. 2 illustrative photos for BRB faults simulated

Table 1 Induction Motor Specification

Rated voltage (Δ/Y)	230/400 V
Rated current (Δ/Y)	15.9/9.2 A
Motor power	4 kW
Number of phases	3
Number of poles	4 poles/phase
Supply frequency	50 Hz
Motor rated speed	1420 rpm
Number of stator slots	36
Number of rotor bars	28
Power factor	0.8

4.3 Data acquisition

Electrical current signals of the testing motor in three phases were measured by a hall-effect sensor with a linear frequency response from DC to 4kHz and measurement range 0 to 50A, which allows the content in a wide frequency range, especially around the supply fundamental of 50Hz, to be measured accurately. A shaft encoder mounted at the free end of the motor was used to measure motor speed and hence the slip changes for confirming the sideband frequency obtained by spectrum analysis.

To examine the influence of the operating condition on fault diagnosis performance, electrical current signals were measured under an increment load cycle from 0%, 25%, 50% to 75% of the full operating load at the rated motor speed. In addition, to perform a sufficient number of averages in MSB estimation and obtain reliable results, the data acquisition was carried out at least three times for the same motor under test through three independent tests each of which repeat the load cycle at the rated speed.

All of the measurements were sampled simultaneously with a high speed data acquisition system at a sampling rate of 96 kHz per channel. This high rate ensures that the speed obtained by the encoder is of sufficient accuracy for slip estimation. The system has a data resolution of 24bits. With this high dynamic data range the small components due to modulation and the large components at supply frequency can be measured concurrently. Moreover, a data length of 20 seconds was acquired for each acquisition in order to achieve a good average in calculating MSB while maintaining sufficient frequency resolution.

5 RESULTS AND DISCUSSION

For evaluation of the signal model and data analysis methods, the datasets of current signals for the baseline and three BRB cases were processed to obtain their corresponding MSBs respectively. The segment size for DFT calculation was set to be 768000 points, attaining a frequency resolution of 0.125Hz for differentiating the small frequency change under low load . A Hanning data window was applied to the data segment to minimize the sidelopes of DFT. In addition, a 40% overlap between segments was used and the number of average was set to more than 100 for effective noise and interference suppression. A single Matlab function was developed to calculate PS, CB and MSB simultaneously according to Eqns.(19), (20) and (21) respectively, which allowed their performance to be compared under the same conditions. With the same calculating parameters the PS and MSB-SE were also calculated for direct comparison.

5.1 Characteristics of MSB

Figure 3 presents typical MSB results under two broken bars. As it can be seen in Figure 3(a) MSB shows two distinctive peaks at bifrequency (2.25,50)Hz and (24.4,50)Hz in the bispectrum domain. Clearly, the first one is relating to the $2sf_s$ and can be relied on to detect and diagnose BRB without doubt, whereas the second one is relating to rotor speed due to the speed oscillation created by inherent misalignments. Besides, these two peaks are also distinctive in MSB coherence in Figure 4(c), confirming that they stem from modulation processes between $2sf_s$ and f_s, and f_r and f_s respectively and that these modulations have good signal to noise ratio.

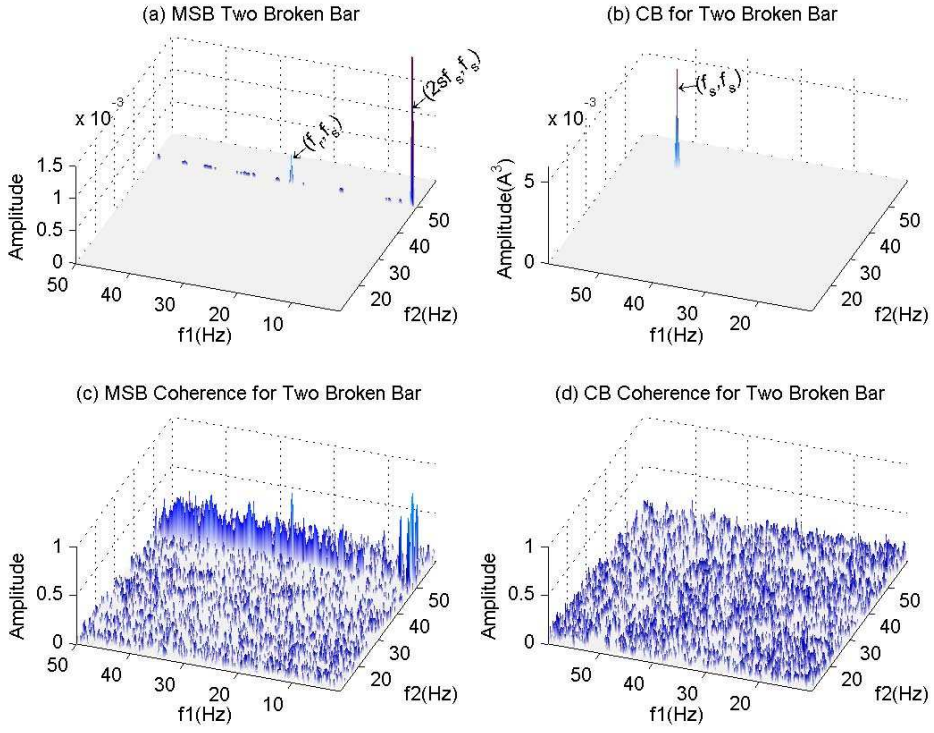

Figure 3 Characteristics of MSB and CB for a two broken bar case under 50% load

On the other hand, the CB in Figure 3(b) shows a single peak at bifrequency (50, 50)Hz. This frequency does not show any connections to BRB at $2sf_s$. Moreover, CB coherence in Figure 3(d) is predominated by background noise in the whole domain of interest. It means that the peak at (50,50)Hz is not from real nonlinear coupling, but is due to the very high amplitudes at 50Hz in the original signal.

To examine further the characteristics of MSB, the behaviour of peaks and their associated phases during the average process in estimating MSB and CB are presented in Figure 4. As can be seen, the

two peaks are from MSB becoming stable as the number of averages increases. In particular, the peak amplitude at $2sf_s$ is nearly stable after a number of averages equal to 60, whereas the amplitude relating to f_r still shows noticeable fluctuation after 60 averages due to its lower signal to noise ratio (SNR). Thus it can be acceptable to estimate MSB with about 100 averages.

Especially, the instantaneous phases shown in Figure 4(d), obtained at each data segment, show that these two MSB components exhibit relatively small fluctuation over different segments, indicating that they are independent of data segments used. In contrast, the phase for the peak at (50,50)Hz from CB shows significantly larger changes between data segments, which leads to the averaged amplitude becoming smaller with the increase of the average number, as shown in Figure 4(c).

It is also worth noting that the phase distribution of data segments is far from the uninform assumption made in developing bispectrum analysis. Therefore, it is suggested that segment sizes and overlaps should be adjusted more than once to ensure phases are distributed differently to avoid any coincidental phase alignment.

In addition, the phase of MSB peak at (24.7, 50)Hz is slightly larger than π. As discussed in Section 3.1 this shows that this modulation is mainly caused by pure speed oscillation. However, because of the influences of the impedance shift it is still not a symmetric phase modulation process. For the similar reason, the MSB phase at bifrequency (2.25,50)Hz is much larger than π, indicating that the modulation is from a more complicated modulation process such as BRB expressed in Eqn. (15). These phase differences can be combined for differentiation of different modulation processes.

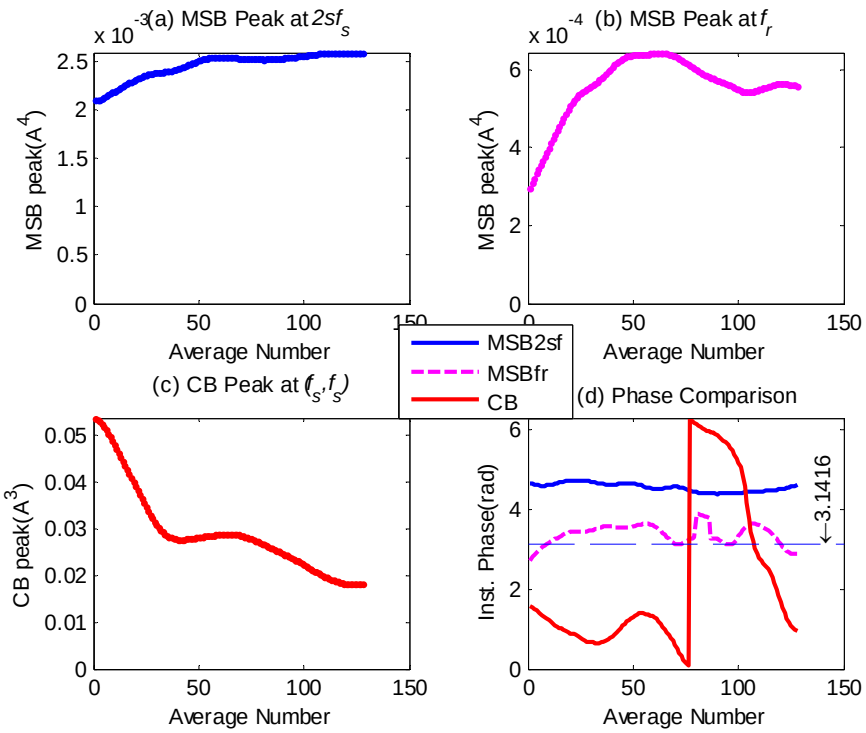

Figure 4 Average process of MSB peaks for two broken bar case under 50% load

Overall, this examination shows that MSB is an effective approach to extracting the small modulation features in motor current signals for rotor fault diagnosis. However, CM is not very suitable to do so.

To show the capability of MSB in suppressing random noise for measured signals, a comparison is made between MSB and PS based on the same data sets above. Figure 5 shows an MSB-SE which is plotted on top of the PS by a frequency shift mirrored about 50Hz. As seen in the graph, the floor noise level of MSB-SE is nearly 10dB lower than that of PS in the frequency range from 0 to 10Hz. Because of the good noise suppression capability, the higher order harmonics of $2sf_s$ can be resolved much more easily. Similarly, the components at f_r and even $2f_r$ can be identified without any difficulty. However, there may be a problem in identifying $2f_r$ by PS because the peak at $(f_s - 2f_r)$ is invisible due to high noise level. This demonstrates that MSB has a good noise reduction capability, which leads to a more accurate amplitude of the modulating components. In addition, Figure 5 also shows that MSB-SE produces a sparse representation of current spectrum. It makes the identification and extraction of fault components much easier and more reliable.

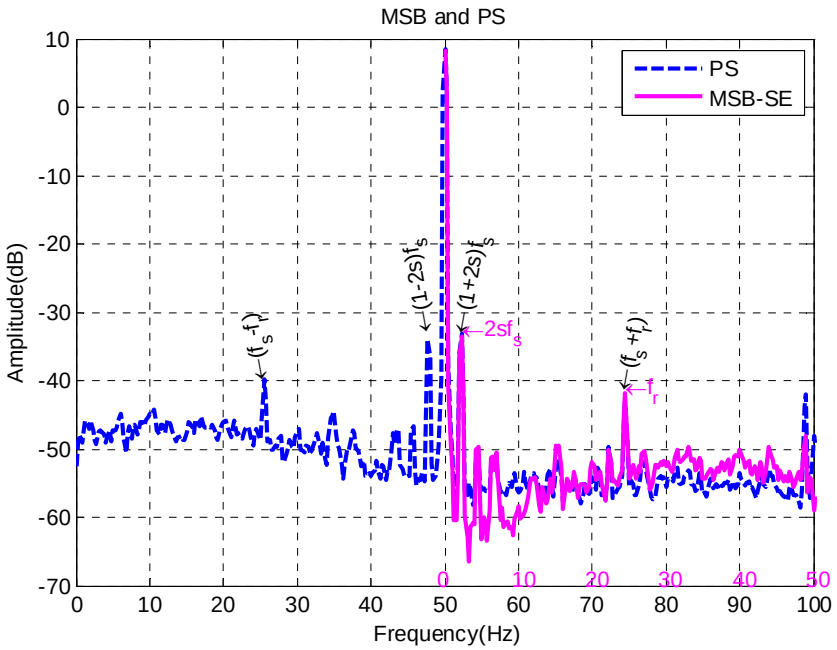

Figure 5 Comparison between MSB and PS for two broken bar case under 50% load

Figure 6 presents peak amplitudes and phases extracted from MSB for different BRB cases and different load conditions. It can be seen in Figure 6(a) that the peak values at $2sf_s$ are different when the load is above 25%, showing that MSB amplitudes can be a good indicator for separating different BRB cases. However, MSB phases are overlapping for different cases and show an almost linear trend decreasing with load. These agree with theoretical analysis made in Section 2 in that the phase is not influenced by BRB, but relating to the power factor and hence the loads.

On the other hand, the peaks at f_r are close to each other for different BRB cases. This shows that the tests have been carried out with good consistency between the four motors tested which need careful alignment during their installations onto the test rig. In addition, there is a decreasing trend of these peaks with load. This is examined due to the nonlinear effects of shaft couplings. As the load increases the effective deformation of rubber coupling elements becomes smaller and hence produces a smaller speed oscillation. As shown in Section 3, its phase is almost constant over loads. However, the motor for the case of half bar breakage may be slightly different in its residual eccentricity which leads to its phase diverging slightly at high loads.

In general, the peak values from MSB show good performance of differentiating BRB cases. However, its load dependent trend makes it inconvenient for BRB severity assessment.

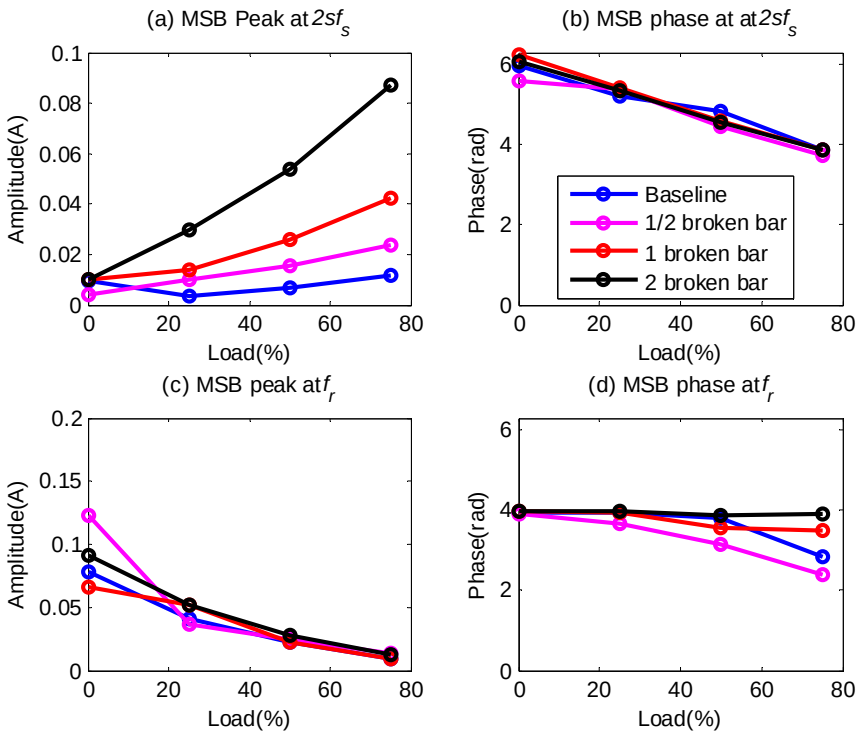

Figure 6 MSB amplitude and phase at 2sfs and fr for different cases and load conditions

5.2 BRB severity diagnosis

To develop a reliable and accurate method for BRB diagnosis, many researches such as those reviewed in [1] and [2], have been carried out in recent years. These have resulted in a number of empirical formulas for estimating the BRB fault severity in terms of the number of broken bars using sideband component amplitudes [12-17]. In general, they used different amplitude ratios between sideband components and fundamental/operating ones which are extracted from conventional spectrum analysis including amplitude spectrum and PS. As already shown in previous sections, the amplitude from normal spectra such as PS may produce an overestimate of the fault because the amplitude includes additive noise. Therefore, to minimize the noise influence on fault severity prediction, the sideband amplitude estimation based on MSB is applied to the data sets.

The second issue is that the decoupling of the lower sideband for the BRB fault current component has not been addressed explicitly in those studies. It often leads to misunderstanding in applying these formulae without performing the decoupling.

Furthermore, the ratios are usually constituted by using the operating current value as the denominator to remove the load dependent trend in severity prediction. It seems that these relationships ignore the fact that the BRB fault current is also influenced by its associated speed oscillation and these

predictions may be just valid for rated operating conditions. Moreover, it is shown by all previous studies that the $(1\pm 2s)f_s$ sideband components only appear when a motor is under load. It means that the BRB fault current amplitude relates only to the active current value, rather than the total operating current. Therefore the denominator of current ratios should only include the effective current rather than the total operating current as suggested in [18].

From these understandings, this study redefines the estimation formula based on works in [14,18]. The current ratio γ is defined as:

$$\gamma = \frac{I_F}{I - I_o} = \frac{n_{brb}}{2N_b - Pn_{brb}} \tag{33}$$

where I is the amplitude of total operating current; I_o is no load current value which can be calculated using the rated power factor and current from motor nameplates, and N_b is the number of rotor bars. This then leads to a direct prediction of the number of BRB:

$$n_{brb} = \frac{2\gamma N_b}{1+\gamma P} \tag{34}$$

More specifically the prediction of the numbers of BRB can be implemented by the following four steps:

1) Using Eqn.(32) in Section 3.3 to minimize noise influences and obtain the denoised amplitudes of both lower sideband and upper sideband;
2) According to the power factor provided on the motor plate to obtain the reactive current value at no-load condition.
3) Using Eqn.(17) to decouple the influences due to speed oscillations and obtain the amplitude of BRB fault current.
4) Using Eqns.(33) and (34) to calculate the number of BRB.

Figure 7 shows the results from sideband estimation by Step 1). As shown in the figure, the proposed method produces a slightly lower estimation, compared with that from PS. The difference is marginal at high loads and severer fault condition because of high SNR signals. However, for the incipient fault case of half BRB and the baseline case, the difference between MSB-SE and PS is significant because of more noise influence, which may lead to incorrect diagnosis by PS analysis.

Figure 8(a) presents the results from Step 3). The values show similar characteristics to that in Figure 7(b) and (c). But they have higher amplitudes, compared with either the lower or upper sideband. It demonstrates that the BRB fault current has been reduced by the interference of the sidebands due to

associated speed oscillations. Because of the difference in fault severity estimation, using either of the sidebands or by their sum, would be inadequate.

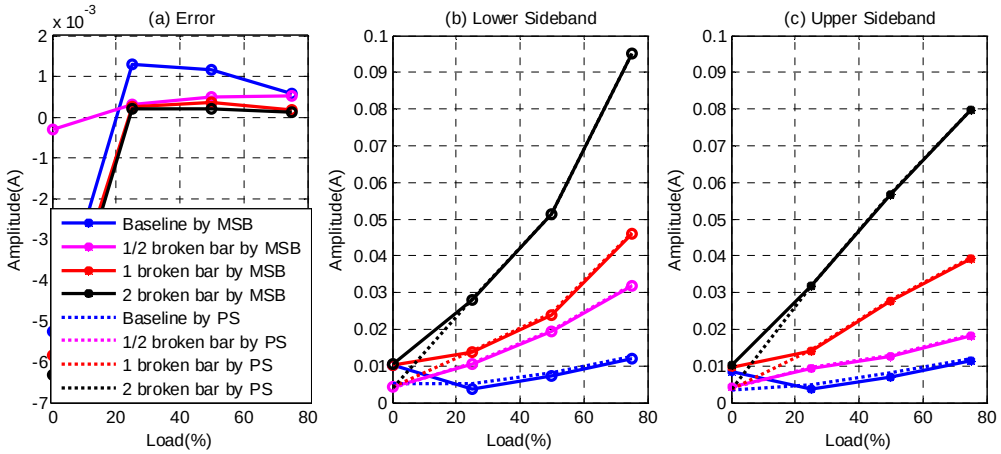

Figure 7 The estimation of sideband amplitudes through MSB-SE for different BRB cases

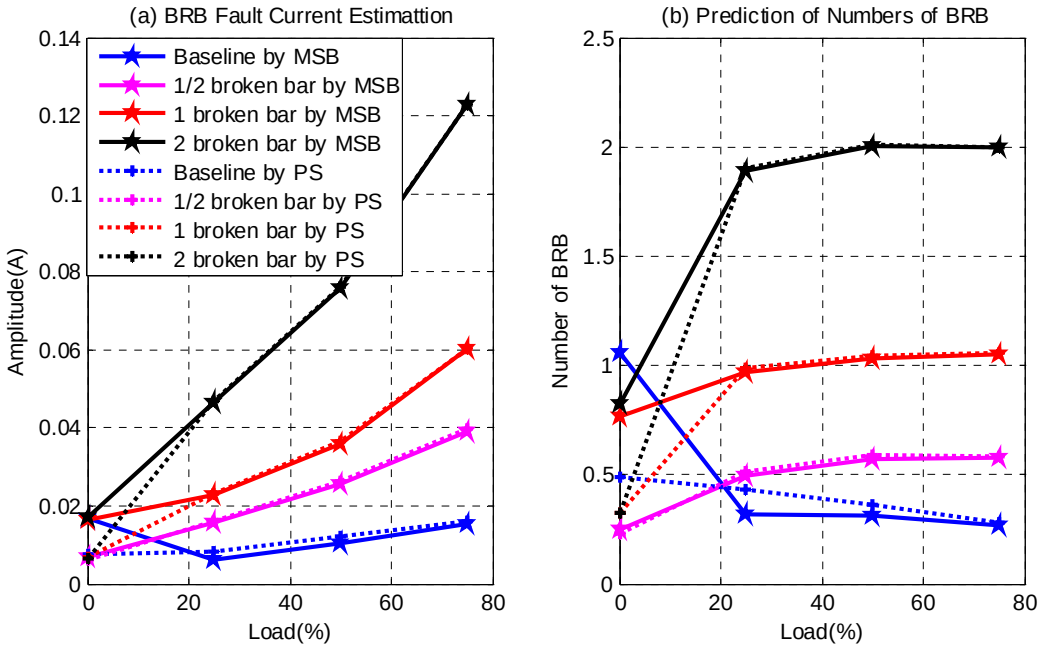

Figure 8 The prediction of BRB current and diagnosis of BRB severity

Having shown the BRB fault currents, the prediction of the numbers of BRB can be carried out and gives results shown in Figure 8(b). It shows that the proposed method gives very close prediction for the tested cases and the results are independent of load conditions, except for the no-load condition. Comparing the results from MSB with that from PS, it can be seen that it is difficult for PS to separate between the baseline and half BRB at load 25% and 50%. However, MSB-SE based results can give

sufficient difference between these cases because it has good noise suppression capability and hence outperforms PS analysis.

6 CONCLUSION

Faults on the rotor of electrical motors cause additional components which modulate the fundamental supply component and lead to a nonlinear phase current signal. In a power spectrum they exhibit as asymmetric sidebands around the supply frequency. To extract these components in noise signals, a new MSB-SE estimator can be applied to measured signals to suppress inevitable noise components and non-modulating components for obtaining a more accurate measure of the modulation. However, the conventional bispectrum is inefficient with respect to this modulation effect in current signals.

For predicting BRB severity, sideband amplitudes at $(1 \pm 2s) f_s$ from PS can be denoised using MSB-SE based, the proposed sideband amplitude estimator and then further decoupled to obtain BRB fault current alone for more accurate prediction of the number of BRB.

Experimental evaluation shows that the new estimators produce more accurate results in predicting the number of BRB under different load conditions and fault cases, compared with power spectrum analysis. Especially it can easily separate the half BRB at a load as low as 25% from baseline where PS would not produce a correct separation.

ACKNOWLEDGEMENT

The authors are grateful for the financial support provided by the National Natural Science Foundation of China under the Grant nos. 51375326 and 51035008

REFERENCES

[1] A. Bellini, F. Filippetti, C. Tassoni, and G.-A. Capolino, “Advances in diagnostic techniques for induction machines,” IEEE Trans. Ind. Electron.,vol. 55, no. 12,2008, pp. 4109–4126..

[2] M. R. Mehrjou, N. Mariun, M. H. Marhaban, N. Misron, Rotor fault condition monitoring techniques for squirrel-cage induction machine—A review, Volume 25, Issue 8, November 2011, pp. 2827–2848.

[3] G. Didier, E.Ternisien, O.Caspary, H.Razik, A new approach to detect broken rotor bars In induction machines by current spectrum analysis, Mechanical Systems and Signal Processing 21(2) ,2007, pp. 1127–1142.

[4] L. Saidi, F.Fnaiech, H.Henao, G-A.Capolino, G.Cirrincione, Diagnosis of broken-bars fault in induction machines using higher order spectral analysis, ISA Transactions 52, 2013, pp140–148.

[5] F. Gu, Y. Shao, N. Hu, A. Naid, A.D. Ball, Electrical motor current signal analysis using a modified bispectrum for fault diagnosis of downstream mechanical equipment, Mechanical Systems and Signal Processing ,Vol. 25, No. 1, 2011, pp 306-372.

[6] M. Haram, T. Wang, F. Gu, A.D. Ball, 'An Investigation of the Electrical Response of A Variable Speed Motor Drive for Mechanical Fault Diagnosis. Proceedings of the 24th International Congress on Condition Monitoring and Diagnostic Engineering Management (COMADEM 2011), COMADEM. 2011, pp. 867-874.

[7] A. Alwodai, , F. Gu, A.D. Ball, 'A Comparison of Different Techniques for Induction Motor Rotor Fault Diagnosis' Journal of Physics: Conference Series , 364, 2012, 1742-6596.

[8] Z. Chen, T. Wang, F. Gu, M. Haram, A.D. Ball, 'Gear Transmission Fault Diagnosis Based on the Bispectrum Analysis of Induction Motor Current Signatures' Journal of Mechanical Engineering , 48 (21),2012, pp. 84-90..

[9] A. Alwodai, Y. Xia, Y. Shao, F. Gu, A.D. Ball, 'Modulation Signal Bispectrum Analysis of Motor Current Signals for Stator Fault Diagnosis'. 18th International Conference on Automation and Computing (ICAC), 2010 . Loughborough, UK, IEEE. 2012, pp. 1-6.

[10] F. Filippetti, G. Franceschini, C. Tassoni, P. Vas, AI Techniques in Induction Machines Diagnosis Including the Speed Ripple Effect. IEEE Transactions on Industry Applications, Vol.. 34, No. 1, Jan/Feb. 1998, pp 98-108.

[11] A.Bellini, F. Filippetti, G. Franceschini, C. Tassoni, G.B. Kliman, Quantitative evaluation of induction motor broken bars by means of electrical signature analysis, IEEE Transactions on Industry Applications Vol.37, No. 5, 2001, pp. 1248–1255.

[12] C. Hargis, B. Gaydon, K. Kamash, The detection of rotor defects in induction motors, in: Proceedings of the IEE Conference Electrical Machine, 1982, pp. 216–220.

[13] R. Hirvonen, On line condition monitoring of defects in squirrel cage motors, in: Proceedings of the International Conference of Electrical Machine (ICEM), 1994, pp.267–272.

[14] W.T. Thomson, On-line Fault Diagnosis in Induction Motor Drives via MCSA, EM Diagnostics Ltd, Scotland, 2001.

[15] W. T. Thomson and M. Fenger, "Case histories of current signature analysis to detect faults in induction motor drives," in Proc. IEEE IEMDC, Jun. 2003, vol. 3, pp. 1459–1465.

[16] F. Filippetti, M. Martelli, G. Franceschini, and C. Tassoni, "Development of expert system knowledge base to on-line diagnosis of rotor electrical faults of induction motors," in Conf. Rec. IEEE IAS Annu. Meeting, Houston, TX, Oct. 1992, pp. 92–99.

[17] H. Jin, N. Faliang, and Y. Jiaqiang, “Using current signature analysis technology to reliably detect cage winding defects in squirrel-cage induction motors,” Front. Elect. Electron. Eng. China, Vol. 2, No. 1,2007, pp. 117–122.

[18] J. Huang, F. Niu, J. Yang, Rotor Fault Diagnosis for Induction Motors Considerring Effects of the Load and Inertia, Proceedings of the CSEE, Vol.26, No.14, July 2006, pp. 120-125.